Available online at www.sciencedirect.com

ScienceDirect

Advances in Space Research 62 (2018) 624–637

ADVANCES IN SPACE RESEARCH
(a COSPAR publication)

www.elsevier.com/locate/asr

Ionospheric response to major storm of 17th March 2015 using multi-instrument data over low latitude station Kolhapur (16.8°N, 74.2°E, 10.6°dip. Lat.)

R.N. Ghodpage [a,*], P.T. Patil [a], O.B. Gurav [b], S. Gurubaran [c], A.K. Sharma [b]

[a] *M.F Radar, Indian Institute of Geomagnetism, Shivaji University Campus, Kolhapur, India*
[b] *Space and Earth Science Laboratory, Department of Physics, Shivaji University, Kolhapur, India*
[c] *Indian Institute of Geomagnetism, Navi Mumbai, India*

Received 2 November 2017; received in revised form 1 May 2018; accepted 3 May 2018
Available online 24 May 2018

Abstract

The optical observations of ionospheric and mesospheric OI 630.0 nm, OI 557.7 nm along with OH emission carried out from low latitude Indian station, Kolhapur (16.8°N, 74.2°E) using CCD based all-sky camera system. The features of night airglow variations observed during the period of a strong geomagnetic storm, which commenced on March 17, 2015, at ∼04:30 UT (10:00 IST (Indian Standard Time = UT + 5.5 h)). Dst of ∼−222 nT was seen in this storm suggest that this is among the strongest. The OI 630.0 nm images on 16, 17 and 18 March show the development of Equatorial Plasma Bubbles (EPBs) and bright intensity regions in OI 630.0 nm emission. Generally, EPBs move from west to east direction but it moved in reverse direction on the strong magnetically disturbed night. The EPBs drift velocity was less by ∼100 m/s than the velocity measured on magnetically quite night 16–17 March 2015. The bright intensity regions are also observed in OI 557.7 nm airglow, but there is no intensity enhancement seen in OH emission. It is also observed that the OI 630.0 nm intensity variation well matches with the GPS VTEC variation for PRN-2. The reversal in EPBs drift velocity and the nightglow intensity variations due to the strong magnetic storm are discussed.

Keywords: Magnetic storm; Ionosphere; EPB; Reverse zonal drift velocity

1. Introduction

Geomagnetic storms are the most important Space Weather phenomena as far as the impact on the global magnetosphere-thermosphere-ionosphere system is concerned. The storm caused by the solar wind energy, captured by the magnetosphere, and transformed, dissipated in the high latitude upper atmosphere through Joule heating/particle precipitation. It affects the composite morphology of the auroral currents, winds, temperature and neutral composition. Subsequently, it causes changes in the mid and low latitudes. The response of the equatorial ionosphere during geomagnetic storms is one of the significant issue related to space weather studies. How geomagnetic storms affect the characteristics of equatorial spread-F and Plasma bubble is an important aspect and has more significance for trans-ionospheric communications. Somewhat large sets of literature now exist to show that at the time of geomagnetic storms and substorms, the ionospheric electric fields, currents and plasma density in the dip equatorial region depart quite significantly on different time-scales from the geo-magnetically quiet time patterns

* Corresponding author.
E-mail addresses: rupeshghodpage@gmail.com (R.N. Ghodpage), ptpiigkop@yahoo.com (P.T. Patil), omgurav91@gmail.com (O.B. Gurav), su.gurubaran@gmail.com (S. Gurubaran), aks_phy@unishivaji.ac.in (A.K. Sharma).

https://doi.org/10.1016/j.asr.2018.05.003
0273-1177/

(Fejer, 1991; Reddy and Nishida, 1992; Sastri et al., 1992a, b; Abdu et al., 1993, 1995; Fejer and Scherliess, 1995). Geomagnetic activity is found to influence preferentially within the zonal, rather than the meridional component of the ionospheric electric field at dip equatorial locations (e.g. Gonzales et al., 1983; Fejer et al., 1985).

The ground-based optical measurements of various F-region and mesospheric night airglow emissions (OI 630.0 nm, 557.7 nm and OH emission) which provide the important information on the response of the ionosphere-thermosphere during the different phases of a geomagnetic storm. Several researchers have brought out the salient features of the F region storm effects by multi-spectral optical observations at equatorial and low latitude stations. Optical and particle measurements made from the ISIS-II spacecraft during August 1972 geomagnetic storm have been reported by Shepherd et al. (1976). They found strong enhancement of thermally produced OI 630.0 nm emission due to plasma heating over two different regions in the magnetosphere during a major storm.

Based on numerous studies, using data from space borne and ground based techniques, it is widely accepted that the OI 630 nm emissions are generated at low latitude F-region heights (~250–300 km). The OI 630 nm emission is closely related to the F- region electron density (Link and Cogger, 1989; Ghodpage et al. 2012) by the following mechanism:

$$O^+ + O_2 \rightarrow O_2^+ + O \quad (1)$$

$$O_2^+ + e^- \rightarrow O\,(^1D) + O \quad (2)$$

$$O\,(^1D) \rightarrow O\,(^3P) + hv\,(630\ nm) \quad (3)$$

Because reaction Eq. (1) dominates the whole process, the production of the OI 630 nm emission is proportional to the molecular oxygen density $[O_2]$ and the oxygen ion density $[O^+]$. The oxygen ion density $[O^+]$ is almost equal to the electron density Ne in the F-layer. Thus, the OI 630 nm emission is a sensitive indicator of the electron density in the bottom side of the F-layer.

However, the major portion of OI 557.7 nm emission comes from the recombination of oxygen atoms in the mesopause region (80–100 km). Some of the studies have focused on the evolution of EPB irregularities under storm-time conditions (Basu et al., 2001; Lee et al., 2002; Su et al., 2002; Kil et al., 2006). For example, Abdu et al. (2003) studied the evolution of equatorial EPBs and found that the disturbed dynamo plays an important role in bubble development during the storm of 26 August 1998 in the Brazilian sector. The westward EPB irregularity could arise from prompt penetration electric field (PPE) in the course of a disturbance sequence lasting several hours. Ma and Maruyama (2006), presented the observations of EPB at mid-latitude detected by a dense GPS (Global Position System) TEC (Total Electron Content) network in Japan and suggested that a prompt penetrating magnetospheric electric field helped to trigger the super bubble. On the basis of multi-instrument observations at middle latitude in the Japanese sector. Sahai et al. (2001) found the small scale intensity depletion structures (with scale size of 30 to 50 km) are caused by possible nonlinear interaction between the medium scale traveling ionospheric disturbances (TIDs) and enhanced regions of the equatorial ionospheric anomaly where, the enhanced ionospheric disturbances were confined at middle latitude during the storm of 12 February 2000. Kiyama et al. (1996); Sahai et al. (2001) have found unusual enhancement of the OI 630.0 nm emission during different phases of magnetic storms at low and mid-latitude stations. In addition, Patra et al. (2016) showed that the generation of EPBs during this period was confined to a narrow longitudinal region between 69° E and 98°E in the Asian sector. Rajesh et al. (2017) studied the all sky camera observations carried out over Taiwan which show the intense EPBs in 630.0 nm airglow images on successive nights of 13–16 March 2015, but the EPBs were absent in the night of 17 March when St. Patrick's Day magnetic storm occurred. Their results show that on the night of the magnetic storm, pre-reversal enhancement of zonal electric field over Taiwan was weaker when compared to that over India. On the other hand, the American sector exhibits a notable increase in Vertical Total Electron Content (VTEC) while in the Asian sector, the largest decrease in VTEC (signatures of EPB structures) is observed (Nava et al., 2016). During storms, the low-latitude ionospheric electric fields can be promptly disturbed by penetrating electric fields. Past studies have shown that average empirical equatorial prompt penetration electric fields are in good agreement with the predictions from global convection models (Fejer and Scherliess, 1997; Fejer and Emmert, 2003). On the other hand, the large variability of these electric fields with different magnitudes and lifetimes is not well understood (Huang et al., 2005). Sahai et al. (1990), presented the first simultaneous optical measurements of the OI 777.4 nm, 630.0 nm and 557.7 nm emissions from Cachoeira Paulista (22.7°S, 45.0°W), Brazil, an equatorial low latitude station and from Fortaleza (3.9°S, 38.4°W), Brazil, an equatorial station, during magnetic disturbances. They found that the dynamic variations in the F region ionospheric parameters were well correlated with the non-diurnal variations observed in the atomic oxygen airglow emissions at both equatorial and low latitudes. Sau et al. (2017) studied the characteristics of equatorial plasma bubbles (EPBs), using OI 630.0 nm emission such as their zonal drift and tilt, from the low-latitude during the main phase of the 17–18 March 2015 storm and observed that the EPBs drifted eastward during 1430 to 1630 UT between 3°S and 15°N dip latitudes.

The motivation to understand the ionospheric responses to geomagnetic disturbances has greatly evolved from academic to practical interests, whereby dedicated government agencies are actively involved in planning and developing strategies to mitigate potential hazards related to intense space weather events (Hapgood, 2012). The aim of the present study is to understand the effect of the storm on ionospheric processes such as F-region airglow emission, Equatorial Spread F (ESF) and Equatorial Ionization Anomaly (EIA). Here we used the OI 630.0 nm, OI 557 nm and OH emission airglow image measurements carried out from Kolhapur (16.8°N, 74.2°E, and dip lat. 10.6°N) during the storm of 17–18 March 2015. GPS and Ionosonde data is also used to support the airglow emission during storm day.

2. Experimental set up

2.1. All sky imager

The all-sky imager (ASI) operating over Kolhapur (16.8°N, 74.2°E, and 10.6°N dip lat.) was developed from Keo-Scientific Limited, Canada. The ASI collects the incoming radiation through a medium format fisheye lens and a set of Plano-convex lenses and monitors OH, OI 557.7 nm and OI 630.0 nm night airglow emissions with the help of high transmission (50–90%) interference filters positioned in a temperature controlled filter wheel. The six filters are constructed up in the filter wheel to allow the transmission of OI 630 nm, OI 557 nm and OH Meinel bands at 720–910 nm and the background at 572.4 nm. The integration times used in the present setup are 120 s, 120 s, 30 s and 120 s, respectively. The front-end optics collects the incoming radiation in 180° field of view (FOV) with a fisheye lens (f/4 Mamiya RB67) that has a focal length of 24 mm and F-ratio of 4. The movement of filter wheel is synchronized with charge coupled device (CCD) detector operation. These operations are computerized with menu driven software. The CCD camera uses a back illuminated 1024 × 1024 pixel CCD (Pixis, ∼ 1 MP resolution) of 24 μm size, 100% fill factor and 16 bit depth. We restrict the image to FOV of 140° to avoid the nonlinearity arising due to curvature effects and also to minimize surrounding lights at lower elevation angles. More details of the ASI and analysis procedure have been explained by Ghodpage et al. (2014) and Patil et al. (2016). Fig. 1 shows the location and FOV of the ASI at ∼250 km altitude which represents the peak emission altitude of OI 630.0 nm night airglow emission.

2.2. Ionosonde at Tirunelveli

To investigate the response on ionosphere during the storm period, we have used the ionosonde data over Tirunelveli (8.71°N, 77.81°E; 0.51°N dip latitude). The Canadian advanced digital ionosonde (CADI) consists of a transmitter, four receivers and two sets of the antenna system. The transmitter unit is capable of operating in the frequency range of ∼1–30 MHz with a peak power of 600 W. The transmitter is a delta dipole antenna, and the receiver antenna array consists of four dipoles arranged in the form of a square (Grant et al., 1995). The pulse length is 40 μs and samples are taken at every 20 μs proving a height resolution of 6 km.

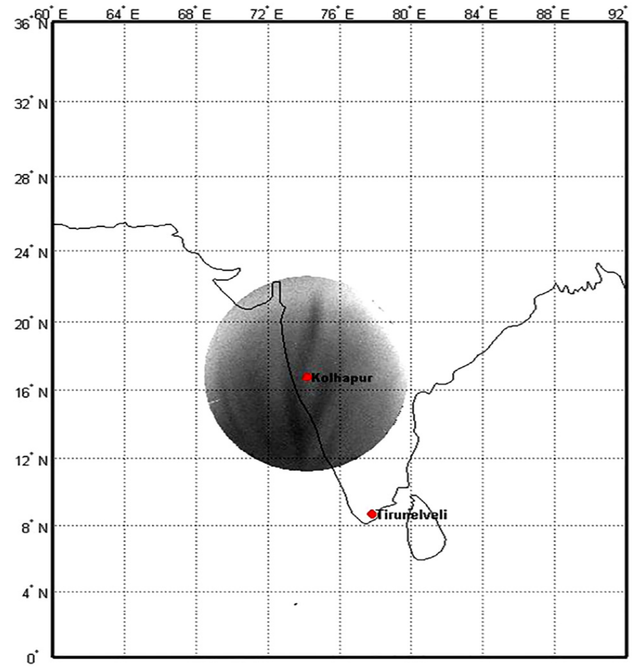

Fig. 1. Circle indicates the area covered by all sky imager having FOV 140°. Center of a circle denotes the location of Kolhapur station. The circular image is nothing but OI 630.0 nm emissions generated at an altitude ∼250 km and captured by ASI onto 1024 × 1024 CCD chip from Kolhapur.

2.3. GPS at Kolhapur

A GSV4004B GPS (Global Positioning System) receiver has been operational at Kolhapur since October 2008. The receiver uses wide bandwidth tracking loops and an internal, phase stable, oven controlled crystal oscillator to compare the phase with the actual carrier phase of GPS observations. Thus, it provides true amplitude, single frequency carrier phase measurements and line of sight code and carrier phase delays on L1 (1575.42 MHz) and L2 (1227.6 MHz) from up to 11 GPS satellites in view, simultaneously and provides outputs in 22 receiver channels. The raw binary data is recorded in the computer and total electron content (TEC) has been estimated using software which reads the RINEX formatted raw data and processes the data for cycle slip correction and phase leveling. Further details are discussed elsewhere (Dashora et al., 2012, Taori et al., 2010).

3. Observations and data analysis

The different emission lines coming from different mesospheric and ionospheric heights can be studied almost simultaneously with the help of this all sky imager system (ASI). Fig. 1 show the location of the observation site on the nights from 16 to 18 March 2015. The geomagnetic storm was in progress on the night of 17 March 2015 at 0445 UT (1015 IST). The geomagnetic field reacted at low latitudes with a relatively strong sudden commencement of nearly 50 nT, followed by a main phase and the peak in Dst of almost −222 nT (Ramsingh et al., 2015). The storm continued up to 0300 UT (0830 IST) in the morning on March 18, the minimum Dst value was reached as −44 nT. The daily solar flux (F10.7 cm) was varying from 113 to 117 (solar flux unit, where 1sfu = 10^{-22} W m^{-2} Hz^{-1}) during this period. Fig. 2 depict the sequence of the processed images of OI 630.0 nm emission observed on the night of March 16–17 (Quit day) at 1802 to 1942 UT (2332 to 0112 IST), March 17–18 at 1805 to 1936 UT (2335 to 0106 IST) and March 18–19 at 1806 to 1945 UT (2336 to 0115 IST, images were covered by clouds). We used an image processing method. The images were taken by all

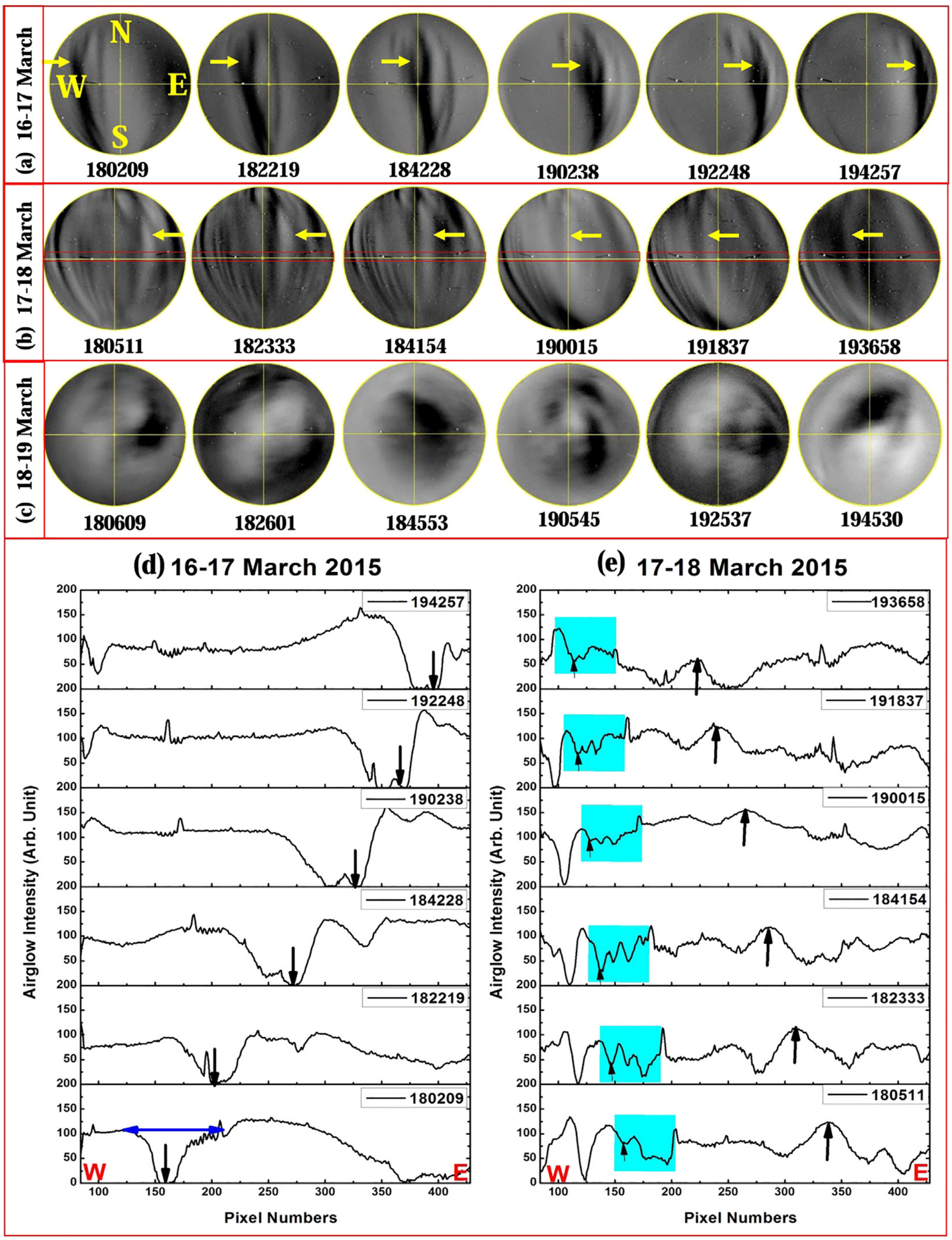

Fig. 2. (a–e) Sequences of processed images for the nights of (a) 16–17, (b) 17–18 and (c) 18–19 March 2015 of 630.0 nm emission recorded using ASI over Kolhapur. (d) and (e) Are the E-W scan plot through zenith for the night of 16–17 and 17–18 March 2015. The downward arrow in figure (d) indicates the propagation of EPB towards East, blue horizontal line is the width of that EPB. The upward arrow in figure (e) indicates the intensity enhancement moving towards west. Also the colored rectangle shows the EPBs with smaller widths as compared to (d). (For interpretation of the references to color in this figure legend, the reader is referred to the web version of this article.)

sky imagers in PNG (Portable Network Graphics) format. Firstly, we read all images collected in one hour and take the average of them and then we subtract this average image from each individual image. After implementing this process we can easily identify the structures of EPBs in OI 630.0 nm images. We draw a circle on images having center at zenith. We divide the images into four quadrants by drawing the horizontal and vertical yellow lines. Then comparing diameter of the image with corresponding original pixel size of the CCD image, we can convert the value of one pixel into kilometer. From Kolhapur, all sky imager covers a horizontal distance of about ~1200 km diameter at an altitude ~250 km. After converting pixel values into corresponding latitude-longitude values of airglow emission height (Narayanan et al., 2009, Taori et al., 2013) and by comparing the longitudinal offset in kilometer of successive images, the zonal velocity of plasma depletions can be easily determined (Pragati Sikha et al., 2010, Ghodpage et al., 2014). Several such plasma depletions marked by yellow arrows could be seen in the images. In Fig. 2(a), the dark regions called EPBs or plasma bubble moves from west to east direction in the sky from 1802 UT on 16–17 March.

Fig. 2(b) depict that after the storm commencement, plasma bubble found to move in a reverse direction (East to West) (1805 to1936 UT) for the night of 17–18 March 2015. Yellow arrows show the motion of intense regions. In Fig. 2(c) unfortunately, the OI 630.0 nm emission images on 18–19 March 2017 (1806 to 1945 UT) were cloudy. Fig. 2(d) and (e) depict the east-west scan of OI 630.0 nm images for the night of 16–17 March 2015 and 17–18 March 2015 at Kolhapur respectively. In Fig. 2(d), the downward arrows represent the propagation of plasma bubble towards east. The horizontal blue line is its width. The average width is measured for the EPB in Fig. 2(d) is ~200 km and for Fig. 2(e) it is ~45 km (for rectangular marked EPBs). The width of the EPBs after reversal is found to be decreased. In Fig. 2(e), the upward black arrows at crest show the enhanced intensity regions (which can also be seen as a bright patch (shown by yellow arrows in Fig. 2(b)) in OI 630.0 nm images on 17–18 March 2015) moving towards west. The colored rectangle is shown in Fig. 2(e) consists of a number of plasma bubbles having smaller widths as compared to plasma bubbles observed on 16–17 March 2015. It is also observed that bright region moves from east to west along with the depletion regions. On 18–19 March 2017, storm goes into the recovery phase, where no major changes could be observed in OI 630.0 nm images.

4. Results and discussion

4.1. Magnetic storm response on airglow emissions

We have used high-resolution airglow images data as explained in the previous section to investigate the effect of the geomagnetic storm over low latitude region. In the east-west scanning of images which is shown in Fig. 2(e), the intensity enhancement is observed before mid-night time (at 1805 UT) and after it tends to decrease with increasing local time. Observation suggests that the OI 630.0 nm intensity variations are characterized by plasma depletions along with enhanced intensity regions, passing over the ASI with local time. Fig. 3(a) represent the sequences of processed images of OI 630.0 nm emission from 1501 to 2032 UT which were observed on the night of 17–18 March 2015 at Kolhapur. The emission intensity was relatively low until 1728 UT, after that it was unusually enhanced. At 1805 UT, the north-east edge of the image started showing enhancement and enhanced area extended to the southward direction covering most of the field of view at 1918 UT. In few images (e.g. 1615 UT, 1551 UT, etc.) we observed unexpected cloud coverage because of which the EPBs are unseen. The white dots in the images are the stars in the night sky. Further, it is very interesting to make a simultaneous measurement of the all-sky imager for the OI 557 nm and hydroxyl (OH) airglow originating at mesospheric height to study the relationship and coupling between MLT (Mesosphere Lower Thermosphere) and the F region during magnetic disturbance. It was clearly observed as shown in Fig. 3(b) that OI 557.7 nm emissions were also significantly enhanced (see 1807 UT) during the period of magnetic disturbance. In Fig. 3 (c), we have seen intensity of hydroxyl (OH) emission remains unaffected during the storm night. Please note that, the white patches seen in the images of OH emission are clouds. Sahai et al. (1990) reported the first simultaneous optical measurements of the OI 777.4 nm, 630.0 nm and 557 nm emissions from Cachoeira Paulista (22.7°S, 45.0°W), in Brazil, a low latitude station and from Fortaleza (3.9°S, 38.4°W) in Brazil, an equatorial station, during magnetic disturbance. The observations of the OI 777.4 nm and 630.0 nm emissions on the disturbed night of 25–26 August at Fortaleza do not show any enhancement when a large enhancement in these emissions at Cachoeira Paulista is evident. Tinsley (1979) reported that, the energetic neutral atom flux might be stronger at low and mid-latitudes and weaker at equatorial latitudes during the main phase of the storm. The moderate geomagnetic activity had considerable effect on the evolution of OI 630.0 nm emission in the low latitude regions while it had no effect on mesospheric emission lines such as Na (589.3 nm) and hydroxyl (OH) emission. The response of the MLT region to geomagnetic activity has generally been not very significant, because the response can be nullified by various internal atmospheric processes such as stratospheric warming, seasonal transitions, atmospheric circulation of waves and local magnetic fluctuations (Balan et al., 2004). The response has been found to be significant during intense magnetic storms ($Kp > 6$) at altitudes above about 90 km (Salah and Goncharenko, 2001; Zhang and Shepherd, 2002, Zhang et al., 2003).

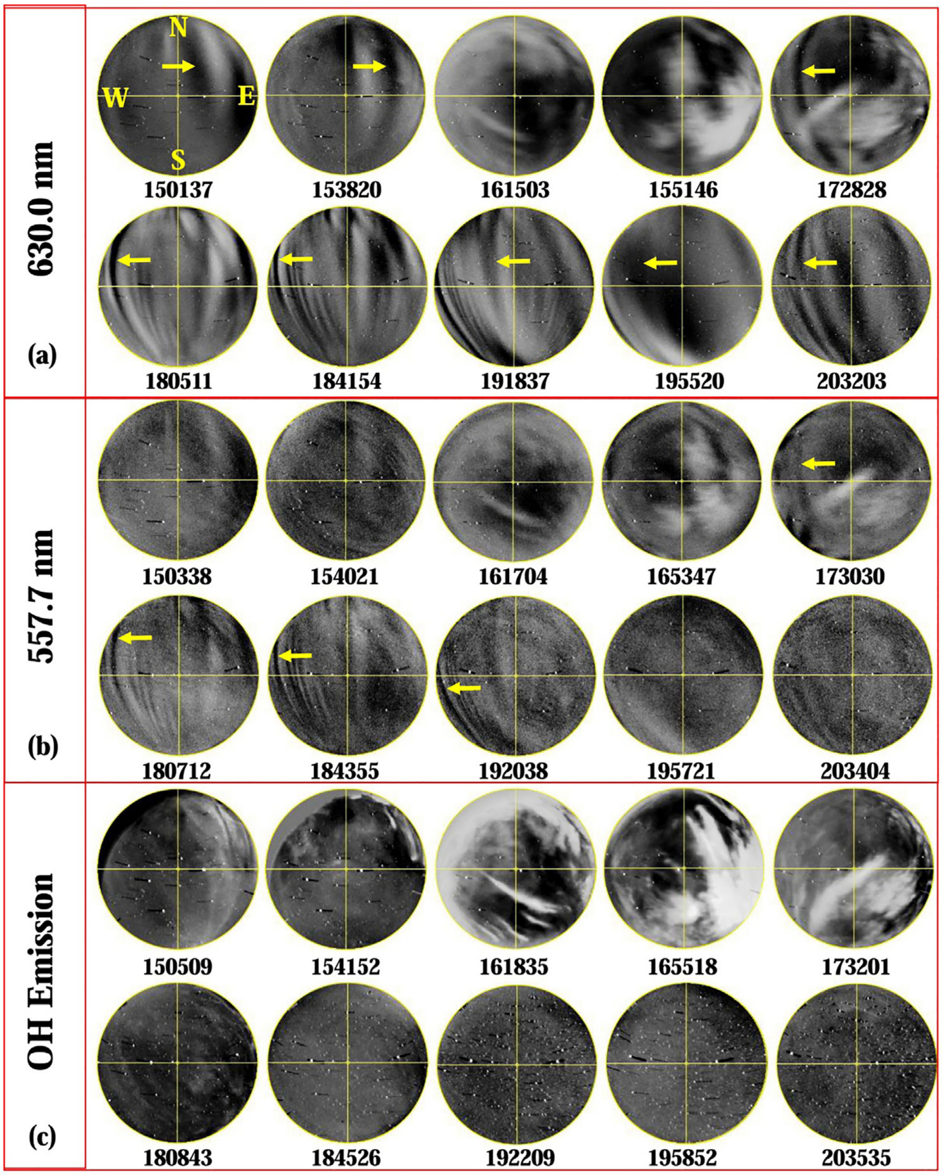

Fig. 3. (a–c) Sequences of processed images for the 630.0 nm, 557.7 nm and OH emissions for the night of 17–18 March 2015 recorded by ASI over Kolhapur.

4.2. Solar and geomagnetic variations and ionosonde observations

The upper panels in Fig. 4(a) and (b) depict the variation of geomagnetic field components (Bz and D) as a function of UT/IST time. The ionospheric response to one of the major storms of the 24th solar cycle which occurred on 17 March 2015, following double halo Coronal Mass Ejections (CMEs) that hit the Earth's magnetosphere at ~0430 UT. Two large eruptions that left the Sun on 15 March 2015 caused this G4 storm. These two Earth directed CMEs added and accelerated together through interplanetary space, resulting into the large geomagnetic storm with DST index decreasing to its minimum of −222 nT. Since, Dst reached −222 nT during this storm period which is the largest of the current solar cycle so far, which can be considered as a super storm here. The information on the magnetic activity during the nights has also been provided in Fig. 4 by hourly Dst and Ap values of magnetic activity indices. On the night of 17 March 2015, the value of Ap index reached maximum as ~175 at 12 UT. In order to understand the ionospheric condition during the period of observation, investigations of ionosphere data (h'F and fof2) from Tirunelveli station (8.71° N, 77.81°E) (Ionosonde data are taken from Ramsingh et al., 2015) has been carried out. Although 16 March is considered as quiet day, as maximum Ap index was just 12, other two days are considered as storm days. The temporal variation of foF_2 and h'F on 16 March show normal behavior and acts as per Equatorial Electro-jet (EEJ) variations. Fig. 4(c) and d represents the foF_2 and base height of the F layer on these 3 days. The F layer of the

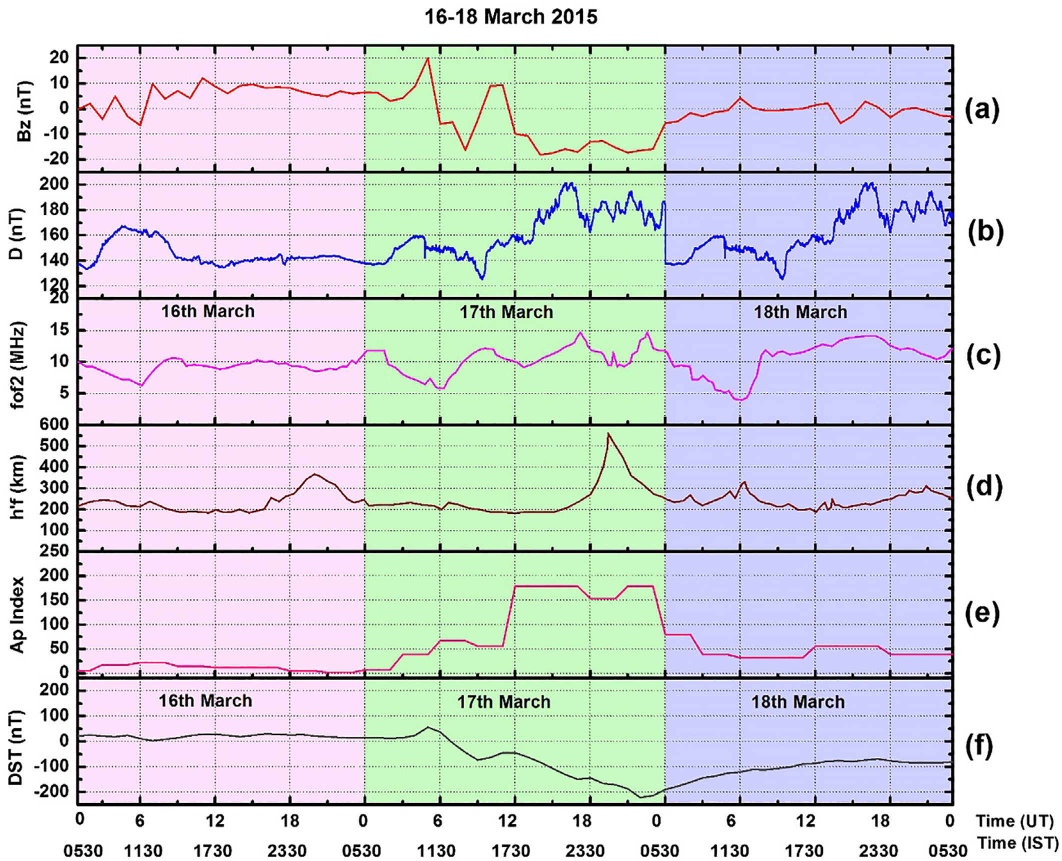

Fig. 4. (a–f) Temporal variations in H (nT), D (nT), fof2 (MHz), h'f (km), Ap index and DST (nT) for the period of 16th to 18th March 2015.

ionosphere responded quite remarkably to the first southward turning of Bz (0600 UT) (at 1130 IST) in terms of height rise of the F layer, and subsequently, the F layer was moving up/down in harmony with Bz. Another effect is the rise in height of the F layer in response to the sudden southward turning of Bz after 1230 UT (1800 IST). The base of the F layer rises up to an altitude of ~550 km, and as a consequence, the density profile of the bottom side F layer turned very steep unlike those on the evenings of 16 and 18 March. It is noticeable that the base height of F layer was larger on 17 March than those observed on 16 and 18 March. On 17 March, the base height of F layer started moving up from ~1430 UT and reached at the peak height of 550 km at ~1900 UT. The base height of the F layer was remained almost at the same height for about 15 min and subsequently started descending. Recovery phase of the storm on 18 March, the post sunset rise of the F layer was remarkably suppressed. However, on the storm day, i.e., 17 March, foF_2 behaved normally up to 0430 UT. Fig. 4(c) and (d) show the time variation of the ionospheric parameters, as the F-layer critical frequency (foF2) and h'f (km) virtual height. Here, the maximum enhancement peaks appeared in between 1600 UT to 2400 UT on the night of 17 March 2015 (Fig. 4(c)). Comparing the period, it is observed that there was also clear enhancement in OI 630.0 nm intensity around this hour (Fig. 2(b)) as enhanced region moving towards west marked as yellow arrows.

4.3. Zonal velocity of EPBs during storm period

Analysis of post sunset observations on 17 March, which are characterized by strong plasma depletions in airglow and also in GPS TEC data. Fig. 5(a) shows the time variations of east-west cross section of OI 630.0 nm airglow images (Keogram) observed from Kolhapur depicting the characteristics and dynamics of bottom side (~250 km) plasma depletions observed on 16–17 March 2015. The calculated zonal velocity measurements on 16–17 March 2017 were shown in Fig. 5(b). Observations show the maximum velocity at ~1600 UT as 170 m/s and it decreases throughout the night and become minimum (~75 m/s) in the morning around 2030 UT. It is interesting to note that the zonal velocity again started increasing from 2030 UT towards dawn. Based on the optical imaging of OI 630.0 nm emission, Patil et al. (2016) reported mean zonal velocity vary between 125 and 160 m/s. Taori and Sindhya (2014) reported that the peak EPB zonal velocity values are 120 m/s, 135 m/s, 160 m/s, and 170 m/s during January, February, April and May 2013 at Gadanki (13.5°N, 79.2°E; 6.5° N dip latitude). Our measurements show the zonal velocity

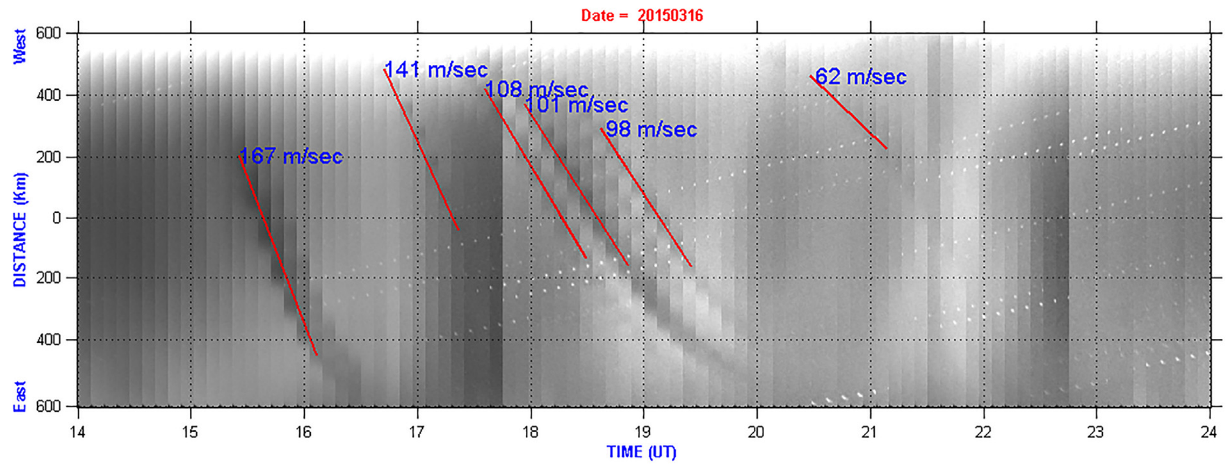

Fig. 5a. Time variations of east–west cross section of 630.0 nm emission airglow images (keogram), illustrating the characteristics and dynamics of bottom side (~250 km) EPB for the night of 16–17 March 2015.

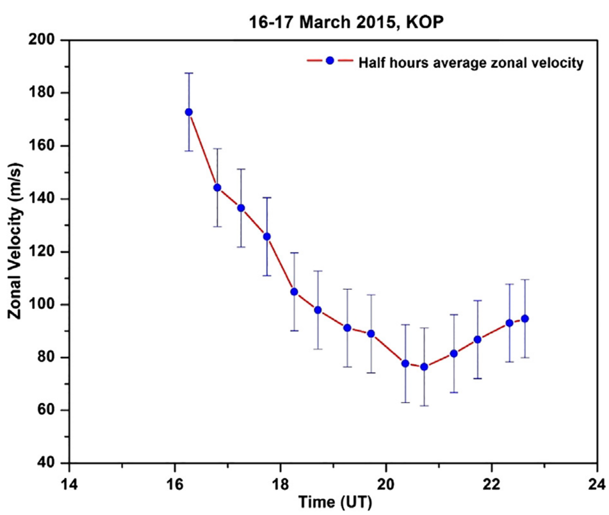

Fig. 5b. Zonal drifts estimated from the movement of the depleted regions observed on 16–17 March 2015 from Kolhapur. The blue vertical line represents the estimated Standard deviation. (For interpretation of the references to color in this figure legend, the reader is referred to the web version of this article.)

varies between 170 m/s and 75 m/s on 16–17 March 2015 which is in agreement with these reports.

In Fig. 5(c), airglow depletion was first detected at 1430 UT (2050 IST). The depleted regions drifted eastward until ~1600 UT (2130 IST) and subsequently drifted westward until the end of the observational campaign (1600 to 2300 UT). It is seen that, the zonal dimensions of the plasma depletions after (2100 UT) were much broader than previous depletions. Fig. 5(d) depicts the calculated zonal drift velocity of the Plasma bubble structures observed by the ASI. The blue line with error bars (standard deviations) represents time variations of zonal drift estimated by using the airglow images. Zonal drift derived from airglow observations, was about ~50 m/s on 1530 UT eastward in the early phase of EPB development, which reduced to zero at 1600 UT (2130 IST) and get reversed afterward with a velocity as high as ~−70 m/s at 1745 UT. EPBs propagate eastward during the night time under quiet magnetic conditions (Taylor et al., 1997, Abdu et al., 2009). However, in recent times, there are reports which suggest that not only geomagnetically disturbed, but also during quiet time conditions, EPBs can drift westward (Otsuka et al., 2012). Patra et al. (2016) also calculated the zonal velocity using OI 630.0 nm images and observed reverse direction of drift velocity ~−90 m/s. Sau et al. (2017) observed westward drift presumably under the influence of the disturbance dynamo electric field initially appeared at higher dip latitudes almost 10 h after the storm onset. The observed zonal velocity derived by Gandanki stations on storm day matches very well with Kolhapur station. Observations at Kolhapur represents that on the storm day EPB zonal velocity is less than quit day zonal velocity. It may be due to the presence of strong disturbed dynamo (DD) on the storm night apart from prompt penetration (PP) electric fields (Ramsingh et al., 2015).

4.4. Storm response on VTEC

Fig. 6(a) depict the vertical TEC fluctuations on 16 to 18 March 2017 as a function of time. Total Electron Content (TEC) was measured continuously from the carrier phase delays (L = L1 − L2) of two GPS signals (L1 = 1575.42 MHz and L2 = 1227.60 MHz) in the ionosphere by using different receivers of the Global Positioning Satellites (GPS). The TEC variations are mapped on the geographical coordinates at an altitude of ~250 km along the line of sight between the ground receiver and the GPS satellites (altitude = ~20,000 km). The temporal variation of GPS (VTEC) from the equator to beyond anomaly crest zone Kolhapur for the period of 16–18 March 2015 is plotted in this figure. Here, it may be mentioned that we have excluded VTEC value whose elevation angle is below 40° (zenith angle 50°). This means that we have plotted the VTEC variations of the PRN's within 50° zenith angle

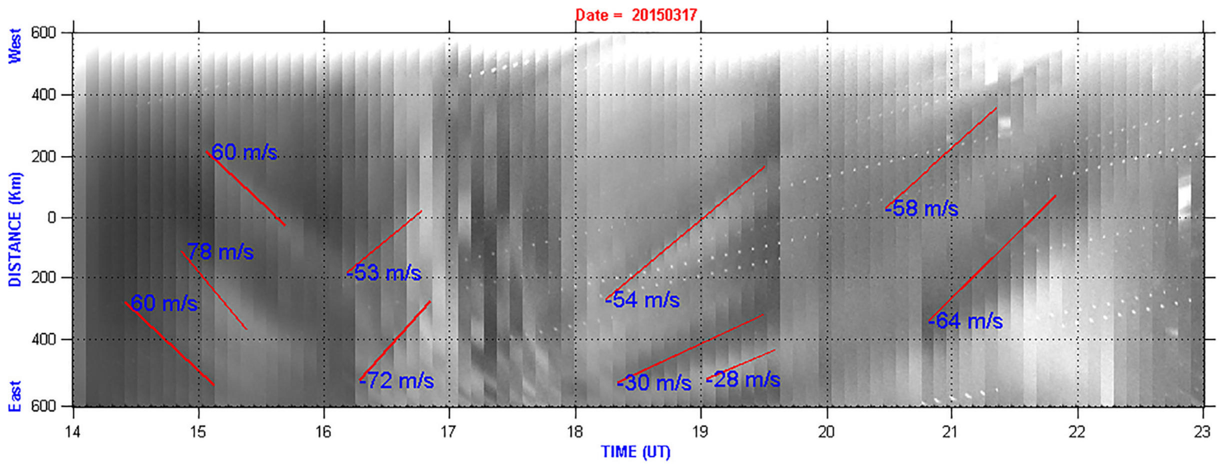

Fig. 5c. Time variations of east–west cross section of 630 nm emission airglow images (keogram), illustrating the characteristics and dynamics of bottom side (~250 km) EPB for the night of 17–18 March 2015.

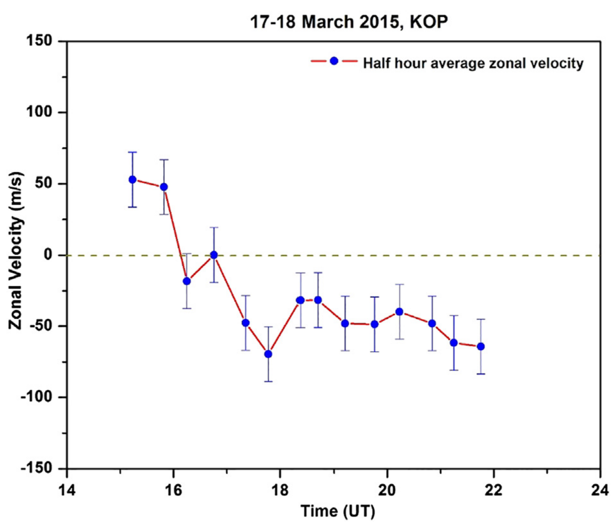

Fig. 5d. Zonal drifts estimated from the movement of the depleted regions observed on 17–18 March 2015 from Kolhapur. The blue line represent estimated Standard deviation. (For interpretation of the references to color in this figure legend, the reader is referred to the web version of this article.)

(100° FOV) from receiver location. This is done to avoid unwanted noise and errors in VTEC due to lower elevation angle. Different colors indicate different PRNs. The maximum TEC value for 16 March 2015 has reached to ~78 TEC unit between 0600 UT to 1200 UT. On 17 March, the Sudden Storm Commencement (SSC) occurred at 0445 UT, the TEC increased between 0800 and 1200 UT. This increase did not see in other two days. Since the GPS receiver has shown these enhancements at day time, these enhancements are believed to be caused by electric field. This happens during the main phase of the storm. Our observations show significant TEC enhancements of ~85 TECU for Kolhapur station at 1000 UT during the storm day as compared to the other two days. It is believed that eastward electric field mapped due to the PP to low latitudes during daytime can push the ionization to higher altitudes through the upward E × B drift where recombination rates are low, causing an additional plasma to be generated by solar illumination, resulting in a net increase of electron density, consistent with our observations. Since the strong Pre-Reversal Enhancement (PRE) drives post sunset anomaly crests at low latitudes, these enhancements could be associated with PRE related to Equatorial Ioniza-

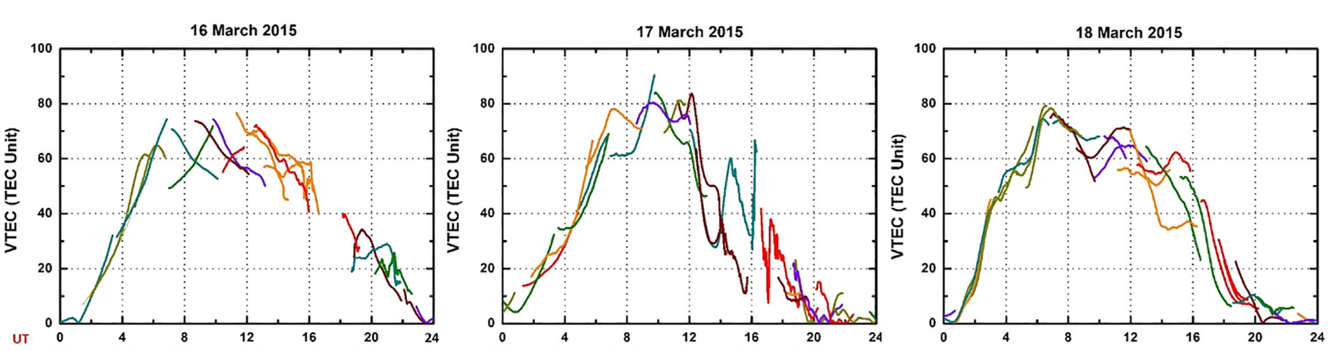

Fig. 6a. Shows the temporal variation in TEC (vertical) during 16–18 March 2015 from Kolhapur station.

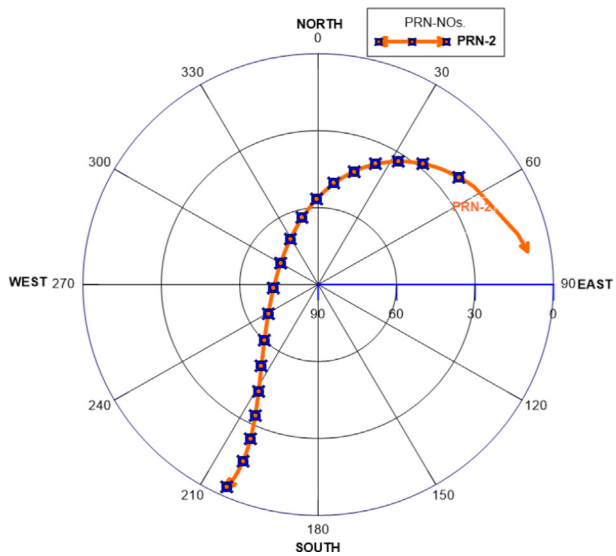

Fig. 6b. GPS (PRN-2) sky plot for Kolhapur on 17–18 March 2015.

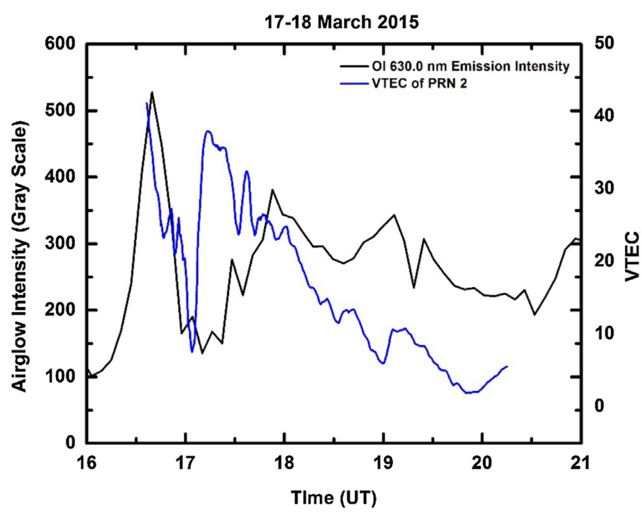

Fig. 6c. Comparison between OI 630.0 nm emission intensity variations with GPS VTEC for the night of 17–18 March 2015.

tion Anomaly (EIA) enhancements. On 18th March, TEC is not prominent as compared to storm day and it varied below ~80 TEC units.

In Fig. 6(b), GPS (PRN-2) sky plot for 17 March 2015 over Kolhapur is shown. Here, PRN-2 is moving from south west to east side in night time when our ASI observation is in progress. PRN-2 moved from nearly to zenith of all sky imager observation site. Hence it is very useful for comparison of OI 630.0 nm emission intensity with PRN-2 VTEC data. Fig. 6(c) depict the comparison of these two data sets. The average intensity of 5×5 pixel rectangle (corresponds to 1° FOV) at zenith is calculated for each image on the night of 17th March 2015 and plotted against time as shown in Fig. 6(c). We observed that GPS VTEC for PRN-2 and OI 630.0 nm emission intensity trend is almost similar and matches well with each other.

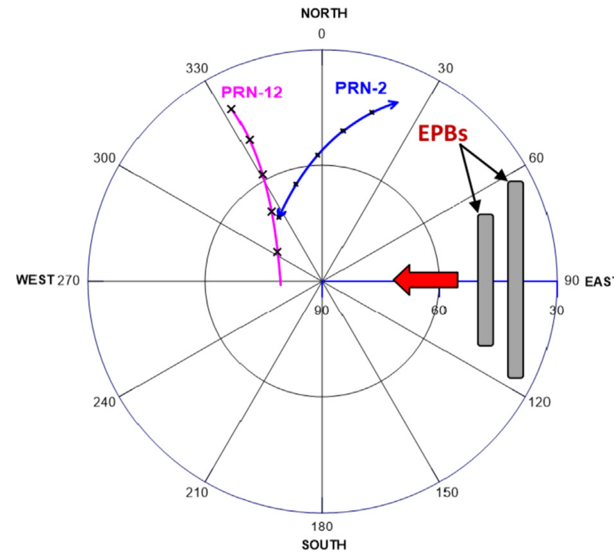

Fig. 6d. Sky plot for PRN-12 and PRN-2 on 17–18 March 2015. The vertical bars (Grey color) shows the schematic of EPBs moving from east to west direction.

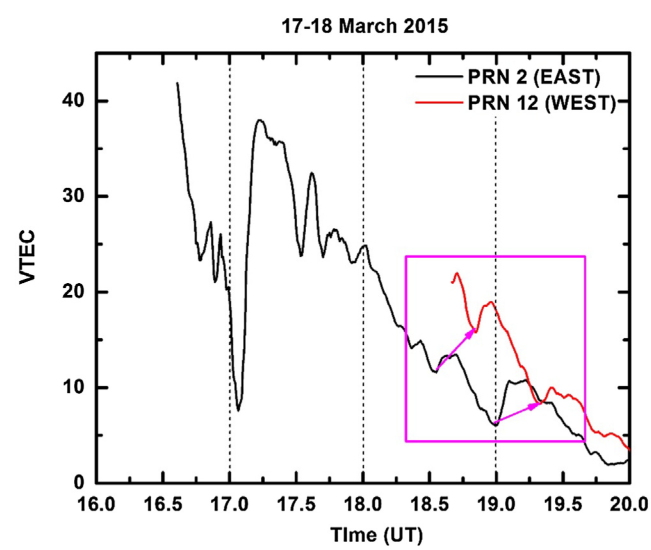

Fig. 6e. The VTEC of PRN-12 and 2 shows the EPBs moving from EAST to WEST direction. The depletions in TEC are the signatures of EPBs shown as arrows in pink rectangle. (For interpretation of the references to color in this figure legend, the reader is referred to the web version of this article.)

This show that plasma bubble observed in ASI images were also observed in VTEC data as depleted TEC (blue curve) and this confirms the EPB presence over Kolhapur station on the night of storm on17–18 March 2015. Fig. 6(d) show GPS sky plot of two PRNs (PRN- 2 and 12) along with plasma bubble (gray colored vertical bars). It is clear that, PRN-2 is moving towards east direction and PRN-12 is moving to west direction, which is useful to check plasma bubble movement. Fig. 6(e) show VTEC values of PRN-2 and PRN-12 and plotted against time. It is observed that the plasma bubble was moving from EAST to WEST direction which is indicated by pink arrows in rectangle. This confirms that the plasma bubble reversal is observed in OI 630.0 nm images (Fig. 3(a)) and is also experienced by GPS PRN-2 and PRN-12 simultaneously.

5. Summary

In this study, the characteristics and dynamics of ionosphere during the period of strong geomagnetic storm, 17 March 2015, from a low latitude station, Kolhapur, India have been studied using both radio (GPS) and optical (ASI) observations. The important features of these observations are as follows:

Enhancement is seen in OI 630.0 nm emission intensity on the night of 17 March during the period of geomagnetic disturbance. Tinsley et al. (1986) found that the intensity variations at low latitude stations are closely related to the magnetic signatures of the storm-time current system and the brightest emissions occur when Dst is large and specifically when positive horizontal magnetic field, H excursions take place. Takahashi et al. (1987) reported that the ionization enhancement occurs at low latitudes during magnetically disturbed conditions. They showed that these enhancements were having an equatorial anomaly like structure with a minimum at the dip equator. Fesen et al. (1989) reported the prominent enhancements of F-region critical frequency in the ionization crest region during disturbed days. In our observation, the ASI images of OI 630.0 nm and 557.7 nm airglow was found to be disturbed during the recovery phase of the storm while the hydroxyl OH emission remained unaffected. The low latitude ionospheric data showed remarkable changes in foF2 values during this period. It is seen that OI 630.0 nm enhancement was confined to low latitude region only. In the mid latitude region, the electron density parameter, TEC, did not show any enhancement or decrease at night. As OI 557.7 nm mesospheric emission receives a small contribution (about 20%) from F-region airglow (Fagundes et al., 1995), if OI 630.0 nm intensity is enhanced during magnetic disturbance, OI 557.7 nm contribution also gets modified proportionally. It is well understood that ground based observations of OI 557.7 nm emission line receive two contributions to the integrated intensity originating from two layers as 90 to 100 km and the F region altitudes ($\sim$ 250 to 300 km). When OI 630.0 nm emission is very intense, F layer component of OI 557.7 nm becomes very much stronger and can dominate the 96 km component significantly. For intense magnetic disturbances, the OI 630.0 nm fluctuations are mainly controlled by sharp changes in height variations of the F-layer (Mukherjee, 2000). Shiokawa et al. (2002) observed intense airglow band in Southern Okinawa in Japan during the period of a geomagnetic storm on 6 August 2000, slowly moving with a velocity of $\sim$40 m/s towards south. This band enhancement seems to correspond to the equatorial anomaly of the ionosphere. The ionosonde observations from low latitude station, Tirunelveli showed the enhancement in electron density (which is proportional to foF2) on the nights of 17th March as compared to 16th March. The discrepancy in airglow enhancement and electron density (obtained from Tirunelveli) during the nights, if any, may be due to the difference in the altitude and position, between the airglow producing layer and F-layer density peak.

A reversal of the normal nighttime downward drift of the F-layer to the upward direction is required to generate large scale irregularities (Aarons, 1991). At night time, zonal westward electric field produces a downward vertical drift. The EPB or depletions were not observed on the night of 18 March 2015. It is generally accepted that the height of the equatorial F layer in the sunset time period is an important parameter controlling the generation of spread-F irregularities. The disturbance dynamo electric field and disturbance zonal wind produced by auroral activity could be responsible for the inhibition of the sunset enhancement of the electric field thereby reducing the height of the F layer. The gradient of electron density before the storm as well as changes in the gradient produced during the storm could also be the deciding factor in the generation of ionospheric plasma irregularities (Sahai et al., 1993).

The GPS-TEC observations at Kolhapur showed enhancements after local noon time maximizing on 17 March 2015 the storm day. The effect was more prominent at Kolhapur station which is situated closer to EIA region. The TEC enhancements may be caused by upward electron motion (fountain) in the low latitude region due to penetration of eastward electric field associated with the storm time sub-storms. This is primarily due to atmospheric effects that create [O]/[N2] enhancements at low latitudes, while [O]/[N2] decreases account for the dominant negative phase effects of the storm at a more pole ward location (Mendillo et al., 2000). This phenomenon is related to the Joule heating in the region of the auroral oval which induces decrease in the ratio [O]/[N2] and correspondingly a decrease in electron density and foF2 in the F2 region. The storm induced disturbed electric fields could account for the major responses. A direct penetration of magnetospheric electric field (often referred to as penetration electric fields) associated with sub storm (asymmetric ring current) development/decay processes can occur in the low latitude equatorial regions and which can produce lowering of the F-region of the ionosphere and subsequent enhancement in OI 630.0 nm emission due to dynamo field modifications. The direction of electric field is very important. Also, the disturbed dynamo electric fields produced by changes in the thermospheric circulation originating from the energy deposition in high latitudes which can produce heating in low latitude ionosphere with time delays of few hours (Sobral et al., 1997). Fig. 6(a) shows enhanced GPS TEC on 17 March 2015. On this night, the EPBs are observed which can be seen as troughs in TEC plot after 1200 UT (1730 IST).

6. Conclusions

The main conclusions of the studies carried out in response to the major geomagnetic storm (17 March 2015) over equatorial and low latitude ionosphere on the 24th solar cycle using All Sky Imager and GPS TEC observations from Kolhapur and ionosonde observation from Tirunelveli are depicted below.

1. The zonal drifts of EPBs turned westward after 16 UT on 17 March instead of usual eastward drift. This indicates the presence of strong disturbance dynamo apart from penetration electric field during this period.
2. The enhancement peaks in electron density can be seen in ionosonde foF2 variation between 1800 UT to 2400 UT on 17 March 2015. This enhancement is also seen in OI 630.0 nm emission all sky images as bright patches moving in the reverse (westward) direction.
3. The westward moving EPBs are also seen in OI 557.7 nm all sky image data along with OI 630.0 nm emission. However, no intensity enhancement was seen in OH emission during the magnetic disturbance.
4. The GPS (VTEC) shows maximum enhancement up to ~85 TEC Unit after local noon time on 17 March 2015. Also, the downward troughs seen in VTEC data on 17 March 2015 indicates the presence of EPBs.
5. The average width measured for the EPBs during 1800 UT to 1930 UT on 16 March 2015 was around ~200 km and it is reduced to ~45 km on 17 March 2015 for the same period. The EPBs on 16 March 2015 were moving eastward and on next day they were moving westward. After the reversal, the width of the EPBs is found to be decreased. This new aspect needs more clarification to understand the morphological behavior in EPBs during such a storm period.
6. It is noticeable that the base height of F layer was larger on 17 March than those observed on 16 and 18 March.

Acknowledgment

The authors thank the Director IIG, Navi Mumbai, for the encouragement to carry out the present work. One of the authors Mr. O.B. Gurav is thankful to UGC-BSR, New Delhi, India for financial support (F.25-1/2014-15(BSR)/7-167/2009/BSR, October 2015). The authors are also grateful to Mr. Rohit Patil for helping in Matlab Programming for ASI Data analysis. The authors are thankful to Dr. Vinit Erram for his useful suggestions during the writing of this manuscript. Thanks are due to the NOAA-GOES for providing the data of solar and geomagnetic indices over the Internet (ftp.swpc.noaa.gov/pub/warehouse). Last but not least, we thank the SPDF, NASA for providing the interplanetary magnetic field (IMF) Bz and Disturbance storm index (DST) data which is available in the public domain (https://omniweb.gsfc.nasa.gov/form/omni_min.html). The night airglow observations at Kolhapur were carried out under the scientific collaboration program (MoU) between IIG and Shivaji University, Kolhapur. Authors wish to thank the anonymous reviewers for their suggestions, which helped to improve the paper.

References

Abdu, M.A., Walker, G.O., Reddy, B.M., de Paula, E.R., Sobral, J.H.A., Fejer, B.G., Szuszczewicz, E.P., 1993. Global-scale equatorial ionization anomaly (EIA) response to magnetospheric disturbances based on the May-June 1987 SUNDIAL coordinated observations. Ann. Geophys. 11, 585–594.

Abdu, M.A., Batista, I.S., Walker, G.O., Sobral, J.H.A., Trivedi, N.B., de Paula, E.R., 1995. Equatorial ionospheric electric fields during magnetospheric disturbance: local time/longitude dependences from recent EITS campaigns. J. Atmos. Terr. Phys. 57, 1065–1083.

Abdu, M.A., Batista, I.S., Takahashi, H., MacDougall, J., Sobral, J.H., Medeiros, A.F., Trivedi, N.B., 2003. Magnetospheric disturbance induced equatorial plasma bubble development and dynamics: a case study in Brazillian sector. J. Geophys. Res. 108 (A12), 1449. https://doi.org/10.1029/2002JA009721.

Abdu, M.A., Batista, I.S., Reinisch, B.W., de Souza, J.R., Sobral, J.H.A., Pedersen, T.R., Medeiros, A.F., Schuch, N.J., de Paula, E.R., Groves, K.M., 2009. Conjugate Point Equatorial Experiment (COPEX) campaign in Brazil: electrodynamics highlights on spread F development conditions and day-to-day variability. J. Geophys. Res. 114, 1–21. https://doi.org/10.1029/2008JA0 13749. A04308.

Aarons, J., 1991. The role of the ring current in the generation or inhibition of equatorial F layer irregularities during magnetic storms. Radio Sci. 26 (4), 1131–1149.

Balan, N., Kawamura, S., Nakamura, T., Yamamoto, M., Fukao, S., Igarashi, K., Maruyama, T., Shiokawa, K., Otsuka, Y., Ogawa, T., Alleyne, H., Watanabe, S., Murayama, Y., 2004. Simultaneous mesosphere/lower thermosphere and thermospheric F region observations during geomagnetic storms. J. Geophys. Res. 109, 120.

Basu, Sunanda, Basu, Santimay, Valladares, C.E., Yeh, H.C., Su, S.Y., MacKenzie, E., Sultan, P.J., Aarons, J., Rich, F.J., Doherty, P., Groves, K.M., Bullett, T.W., 2001. Ionospheric effects of major magnetic storms during the International Space Weather Period of September and October 1999: GPS observations, VHF/UHF scintillations and in situ density structures at middle and equatorial latitudes. J. Geophys. Res. 106 (30389-30), 413. https://doi.org/10.1029/2001JA001116.

Dashora, N., Taori, A., Patra, A.K., 2012. Multi instrument observation of winter solstice F-region irregularities during the low solar activity. Ind. J. Radio Space Phys. 41, 220–232.

Fagundes, P.R., Sahai, Y., Takahashi, H., 1995. Investigations of OI 557.7 nm and 630 nm nightglow intensity ratios during the occurrence of equatorial F-region plasma bubbles. J. Atmos. Terr. Phys. 57 (8), 929–932.

Fejer, B.G., Kudeki, E., Farley, D.T., 1985. Equatorial F-region zonal plasma drifts. J. Geophys. Res. 90, 12249–12255.

Fejer, B.G., 1991. Low-latitude electrodynamic plasma drifts: a review. J. Atmos. Terr. Phys. 53, 677–693.

Fejer, B.G., Scherliess, L., 1995. Time-dependent response of equatorial ionospheric electric fields to magnetospheric disturbances. Geophys. Res. Lett. 22, 851–854.

Fejer, B.G., Scherliess, L., 1997. Empirical models of storm time equatorial zonal electric fields. J. Geophys. Res. 102, 24047–24056. https://doi.org/10.1029/97JA02164.

Fejer, B.G., Emmert, J.T., 2003. Low-latitude ionospheric disturbance electric field effects during the recovery phase of the 19–21 October

1998 magnetic storm. J. Geophys. Res. 108 (A12), 1454. https://doi.org/10.1029/2003JA010190.

Fesen, C.G., Crowley, G., Roble, R.G., 1989. Ionospheric effects at low latitudes during the March 22, 1989, geomagnetic storm. J. Geophys. Res. 94, 5405–5417.

Ghodpage, R.N., Taori, A., Patil, P.T., Gurubaran, S., Sripathi, S., Banola, S., Sharma, A.K., 2014. Simultaneous optical measurements of equatorial plasma bubble (EPB) from Kolhapur (16.81°N, 74.21°E) and Gadanki (13.51°N, 79.21°E). J. Atmos. Terr. Phys. 121, 196–205. https://doi.org/10.1016/j.jastp.2014.05.008i.

Ghodpage, R.N., Siingh, Devendraa, Singh, R.P., Mukherjee, G.K., Vohat, P., Singh, A.K., 2012. Tidal and gravity waves study from ground based optical measurements at low latitude, Kolhapur (India). J. Earth Syst. Sci. 121 (6), 1511–1525. https://doi.org/10.1007/s12040-012-0240-4.

Gonzales, C.A., Kelley, M.C., Behnke, R.A., Vickery, J.F., Wand, R.H., Holt, J., 1983. On the latitudinal variations of the ionospheric electric field during magnetospheric disturbances. J. Geophys. Res. 88 (9135–9143), 1983.

Grant, I.F., MacDougall, J.W., Ruohoniemi, J.M., Bristow, W.A., Sofko, G.J., Koehler, J.A., Danskin, D., Andre, D., 1995. Comparison of plasma flow velocities determined by the ionosonde Doppler drift technique, Super DARN radars, and patch motion. Radio Sci. (USA) 30, 1537–1549.

Hapgood, M.A., 2012. Prepare for the coming space weather storm. Nature 484, 311–313. https://doi.org/10.1038/484311a.

Huang, C.S., Foster, J.C., Kelley, M.C., 2005. Long-duration penetration of the interplanetary electric field to the low-latitude ionosphere during the main phase of magnetic storms. J. Geophys. Res. 110, A11309. https://doi.org/10.1029/2005JA011202.

Kil, H., Paxton, L.J., Su, S.Y., Zhang, Y., Yeh, H., 2006. Characteristics of the storm-induced big bubbles (SIBBs). J. Geophys. Res. 111, A10308. https://doi.org/10.1029/2006JA011743.

Kiyama, Y., Kita, K., Iwagami, N., Ogawa, T., 1996. Atomic oxygen 630 nm and OH Airglows at Mt. Haleakala, Hawaii in February and November 1993. J. Geomag. Geoelectr. 48, 337–341.

Lee, J.J., Min, K.W., Kim, V.P., Hegai, V.V., Oyama, K.I., Rich, F.J., Kim, J., 2002. Large density depletions in the nighttime upper ionosphere during the magnetic storm of July 15, 2000. Geophys. Res. Lett. 29 (3), 1032. https://doi.org/10.1029/2001GL013991.

Link, R., Cogger, L.L., 1989. A reexamination of the OI 6300-A nightglow. J. Geophys. Res. 93, 9883–9892, correction on J. Geophys. Res., 94, 1556.

Ma, G., Maruyama, T., 2006. A super bubble detected by dense GPS network at East Asian longitudes. Geophys. Res. Lett. 33, L21103. https://doi.org/10.1029/2006GL027512.

Mendillo, M., Bosheng, L., Aarons, J., 2000. The application of GPS observations to equatorial aeronomy. Radio Sci. 35 (3), 885–904.

Mukherjee, G.K., 2000. Airglow and other F-layer variations in the Indian sector during the geomagnetic storm of February 5–7. Earth Planets Space. 58, 623–632.

Narayanan, V.L., Gurubaran, S., Emperumal, K., 2009. Imaging observations of upper mesospheric nightglow emissions from Tirunelveli (8.71°N). Indian J. Radio Space Phys. 38, 150–158.

Nava, B., Rodríguez-Zuluaga, J., AlazoCuartas, K., Kashcheyev, A., Migoya-Orué, Y., Radicella, S.M., Amory-Mazaudier, C., Fleury, R., 2016. Middle- and low-latitude ionosphere response to 2015 St. Patrick's Day geomagnetic storm. J. Geophys. Res. Space Phys. 121, 3421–3438. https://doi.org/10.1002/2015JA022299.

Otsuka, Y., Shiokawa, K., Nishioka, M., Effendy, 2012. VHF radar measurements of post-midnight F-region field-aligned irregularities over Indonesia during solar minimum. Ind. J. Radio Sp. Phys. 41, 199–207.

Patra, A.K., Chaitanya, P.P., Dashora, N., Sivakandan, M., Taori, A., 2016. Highly localized unique electrodynamics and plasma irregularities linked with the 17 March 2015 severe magnetic storm observed using multitechnique common-volume observations from Gadanki, India. J. Geophys. Res. Space Phys. 121 (11518–11), 527. https://doi.org/10.1002/2016JA023384.

Pragati Sikha, R., Parihar, N., Ghodpage, R., Mukherjee, G.K., 2010. Observations of gravity waves in the upper mesosphere region by near infrared airglow imaging. Curr. Sci. 98 (3), 392–397.

Rajesh, P.K., H. Lin, Charles., Chen, C.H., Lin, J.T., Matsuo, Tomoko, Chou, M.Y., Chen, W.H., Chang, M.T., You, C.F., 2017. Equatorial plasma bubble generation/inhibition during 2015 St. Patrick's Day storm. Space Weather. 15, 1141–1150. http://doi.org/10.1002/2017SW001641.

Patil, P.T., Ghodpage, R.N., Taori, A.K., Patil, R.P., Gurubaran, S., Nikte, S.N., Nade, D.P., Sharma, A.K., Banola, S., Narayanan, V.L., Siingh, D., 2016. The study of equatorial plasma bubble during January to April 2012 over Kolhapur (India). Ann. Geophys. 59. https://doi.org/10.4401/ag-6868.

Ramsingh, Sripathi, S., Sreekumar, S., Banola, S., Emperumal, K., Tiwari, P., Kumar, B.S., 2015. Low-latitude ionosphere response to super geomagnetic storm of 17/18 March 2015: results from a chain of ground-based observations over Indian sector. J. Geophys. Res. Space Phys. 120, 10864–10882. http://doi.org/10.1002/2015JA021509.

Reddy, C.A., Nishida, A., 1992. Magnetospheric sub-storms and night-time height changes of the F2 region at middle and low latitudes. J. Geophys. Res. 97, 3039–3061.

Sastri, J.H., Ramesh, K.B., Karunakaran, D., 1992a. On the nature of sub-storm related transient electric field disturbances in the equatorial ionosphere. Planet. Space Sci. 40, 95–103.

Sastri, J.H., Ramesh, K.B., Rao, H.N.R., 1992b. Transient composite electric field disturbances near dip equator associated with auroral substorms. Geophys. Res. Lett. 19, 1451–1454.

Sahai, Y., Bittencourt, A., Takahashi, H., Teixera, N.R., Tinsley, B.A., Rohrbaugh, R.P., 1990. Analysis of storm- time low latitude simultaneous ionospheric and nightglow emission measurements. J. Atmos. Terr. Phys. 52 (9), 749–757.

Sahai, Y., Aarons, J., Mendillo, M., Takahashi, H., Abdu, M.A., da Paula, E.R., 1993. Studies of storm-time equatorial F-region irregularities. In: Proceedings of COSPAR Colloquium on Low-Latitude Ionospheric Physics held in Taipei, Taiwan, 9–12 November.

Sahai, Y., Shiokawa, K., Otsuka, Y., Ihara, C., Ogawa, T., Igarashi, K., Miyazaki, S., Saito, A., 2001. Imaging observations of mid-latitude ionospheric disturbances during the geomagnetic storm on February 12, 2000. J. Geophys. Res. 106, 24481–24492.

Salah, J.E., Goncharenko, L.P., 2001. Search for geomagnetic storm effects on lower thermospheric winds at mid-latitudes. J. Atmos. Sol. Terr. Phys. 63, 951–963.

Shepherd, G.G., Cogger, L.L., Burrows, J.R., 1976. Mid latitude Auroral and SAR Arcs observed from the ISIS-II Spacecraft during the August 1972 geomagnetic storm. J. Geophys. Res. 81 (25), 4597–4602.

Sobral, J.H.A., Abdu, M.A., Gonzalez, W.D., Tsurutani, B.T., Batista, I. S., Clua de Gonzalez, A.L., 1997. Effects of intense storms and substorms on the equatorial ionosphere/thermosphere system in the American sector from ground-based and satellite data. J. Geophys. Res. 102 (A7), 14305–14313.

Shiokawa, K., Otsuka, Y., Ejiri, M.K., Sahai, Y., Kadota, T., Ihara, C., Ogawa, T., Igarashi, K., Miyazaki, S., Saito, A., 2002. Imaging observations of the equator ward limit of mid latitude travelling ionospheric disturbances. Earth Planets Space 54, 57–62.

Su, S.Y., Yeh, H.C., Chao, C.K., Heelis, R.A., 2002. Observation of a large density dropout across the magnetic field at 600 km altitude during the 6–7 April 2000 magnetic storm. J. Geophys. Res. 107 (A11), 1404. https://doi.org/10.1029/2001JA007552.

Sukanta, S., Narayanan, V.L., Gurubaran, S., Ghodpage, Rupesh N., Patil, P.T., 2017. First observation of interhemispheric asymmetry in the EPBs during the St. Patrick's Day geomagnetic storm of 2015. J. Geophys. Res. Space Phys. 122. https://doi.org/10.1002/2017JA024213.

Taori, A., Dashora, N., Raghunath, K., Russell III, J.M., Mlynczak, M. G., 2010. Simultaneous mesosphere-thermosphere-ionosphere parameter measurements over Gadanki (13.5°N, 79.2°E): first results. J. Geophys. Res. 116, A07308. https://doi.org/10.1029/2010JA016154.

Taori, A., Jayaraman, A., Kamalakar, V., 2013. Imaging of mesosphere-thermosphere airglow emissions over Gadanki (13.51°N, 79.21°E)-first results. J. Atmos. Sol-Terr. Phys. 93, 21–28. https://doi.org/10.1016/j.jastp.2012.11.007.

Taori, A., Sindhya, A., 2014. Measurements of equatorial plasma depletion velocity using 630 nm airglow imaging over a low latitude Indian station. J. Geophys. Res. 119, 1–6. https://doi.org/10.1002/2013JA019465.

Takahashi, T., Oya, H., Watanabe, S., 1987. Ionospheric disturbances induced by storm associated electric fields in the low latitude F-region. J. Geomag. Geoelectr. 39, 187–209.

Tinsley, B.A., 1979. Energetic neutral atom precipitation during magnetic storms: optical emission, ionization and energy deposition at low and middle latitudes. J. Geophys. Res. 84, 1855–1864.

Tinsley, B.A., Rohrbaugh, R.P., Rassoul, H., Sahai, Y., Teixeira, N.R., Slater, D., 1986. Low latitude aurora and storm time currents. J. Geophys. Res. 91, 11257–11269.

Taylor, M.J., Eccles, J.V., Belleand, J.La., Sobral, H.A., 1997. High resolution OI (630 nm) image measurements of F-region depletion drifts during the Guara campaign. Geophys. Res. Lett. 24, 1699–1702.

Zhang, S.P., Shepherd, G.G., 2002. Neutral winds and O (1 S) emission rates in the lower thermosphere as measured with WINDII/UARS during the April 4–5th 1993 and February 1994 geomagnetic storms. J. Atmos. Sol. Terr. Phys. 64, 1201–1214.

Zhang, S.P., Salah, J.E., Mitchell, N., Singer, W., Murayama, Y., Clark, R.R., van Eyken, A., Thayer, J., 2003. Response of the mesosphere wind at high latitudes to the April 2002 space storm. Geophys. Res. Lett. 30 (23), 2225–2226.